Original Article

Identification and validation of Cystatin A as a novel promising therapeutic target for gastric cancer

Qingyu Xu, Shuai Xue, Yaqiong Zhang, Jian Li, Peiyu Qian, Yanyan Zhang, Li Feng

Endoscopy Center, Minhang Hospital Affiliated to Fudan University, Shanghai, China

Contributions: (I) Conception and design: Q Xu, L Feng; (II) Administrative support: L Feng; (III) Provision of study materials or patients: S Xue; Y Zhang; (IV) Collection and assembly of data: J Li, Y Zhang; (V) Data analysis and interpretation: Q Xu; P Qian; (VI) Manuscript writing: All authors; (VII) Final approval of manuscript: All authors.

Correspondence to: Li Feng, MD. Endoscopy Center, Minhang Hospital Affiliated to Fudan University, 170 Xinsong Road, Shanghai 200000, China. Email: 731810511@qq.com.

Background: The effect of pharmacological treatment of gastric cancer (GC) is limited, thus, it holds significant scientific importance to thoroughly investigate the molecular mechanisms underlying GC development and identify novel molecules capable of substantially extending patients' survival. This study utilized bioinformatics techniques to identify 11 genes associated with recurrence-free survival (RFS) in GC patients and investigated the potential biological functions of these genes through single-cell transcriptomic analysis. Subsequently, a single gene Cystatin A (CSTA) was selected for further analysis to explore its impact on signaling pathways and treatment.

Methods: Differentially expressed genes (DEGs) were identified and overlapped in the analysis of RFS to identify potential prognostic genes for GC patients, based on data from the Cancer Genome Atlas-stomach adenocarcinoma (TCGA-STAD) and GSE54129. Subsequently, a prognostic model based on RFS in GC patients was established. Single-cell sequencing data were employed to explore the potential functions of these model genes. CSTA, one of the RFS-related genes, was further investigated using immunohistochemistry (IHC), Cell Counting Kit 8 (CCK-8), transwell, scratch, colony formation assays, flow cytometry, and Western blotting methods.

Results: Through bioinformatics analysis, we identified 23 RFS-related genes in GC. Using the least absolute shrinkage and selection operator (LASSO)-Cox method, an RFS prognostic model was developed which pinpointed 11 GC prognosis-related (GPR) genes as significant factors influencing RFS in GC patients. The single-cell analysis revealed their potential role in affecting differentiation and maturation of pre-fibroblasts thereby impacting RFS in GC patients. CSTA exhibited low expression levels in GC tissues. Overexpression of CSTA promoted apoptosis in GC cells through the caspase-dependent apoptotic pathway and enhanced their response to cisplatin via this same pathway.

Conclusions: The 11 GPR genes are primarily enriched within a specific type of stromal cell exhibiting heightened communication, metabolism, and differentiation levels. The gene signature of these stromal cells has implications for patient prognosis. Additionally, CSTA, a gene related to prognosis, has been shown to influence apoptosis levels in GC cells.

Keywords: Gastric cancer (GC); Cystatin A (CSTA); tumor microenvironment (TME); prognosis

Submitted May 27, 2024. Accepted for publication Jun 24, 2024. Published online Jun 27, 2024.
doi: 10.21037/jgo-23-941
View this article at: https://dx.doi.org/10.21037/jgo-23-941

Introduction

Gastric cancer (GC) is a prevalent global malignancy, consistently ranking among the top five most frequently diagnosed cancers worldwide each year. It is estimated that over 1 million new cases of GC are diagnosed annually and that it is the third leading cause of cancer-related death globally (1,2). Data from most countries indicate that drug treatments for GC include chemotherapy, targeted therapy, and immunotherapy, among other modalities (3,4).

Chemotherapy has been shown to improve the survival of patients (5,6). The median overall survival of GC patients who receive combination chemotherapy regimens is approximately 1 year (7,8). Approximately 17–20% of GC patients are human epidermal growth factor receptor 2 (HER2)-positive (9). HER2-positive cancer patients can benefit from targeted therapy with HER2 monoclonal antibodies. However, neither pertuzumab (first-line) nor trastuzumab-emtansine (second-line) treatments have been shown to effectively improve survival in GC patients with high HER2 expression (8). Immune checkpoint inhibitors have been used in the treatment of chemotherapy-refractory GC patients who experience tumor progression after first- or second-line therapy. Results from the phase III ATTRACTION-2 trial showed improved overall survival in Asian patients treated with the anti-programmed cell death protein-1 (PD-1) monoclonal antibody nivolumab (10,11). In the current GC treatment landscape, such drugs have limited biological efficacy and significant side effects, thereby, not as a first-line treatment for GC.

The above-mentioned drug therapies for GC all have their own limitations. Therefore, it is of great scientific significance to explore the molecular mechanisms of GC development in depth and search for new molecules that can significantly prolong the survival period of patients. Recurrence-free survival (RFS) refers to the time from complete remission after anti-tumor treatment until recurrence or the end of follow-up. Longer RFS after anti-tumor treatment indicates better treatment efficacy (12-14). In our quest to identify novel molecules with potential impact on the RFS of GC patients, we employed bioinformatics and discovered that Cystatin A (CSTA) expression exerts a positive influence on patient survival.

CSTA, a member of the cysteine proteinase inhibitor superfamily located on chromosome 3q21.1, is involved in late-stage keratinocyte differentiation and has long been implicated in cell adhesion (15,16). Recent findings demonstrate decreased CSTA expression in cancer tissues, while showing an association with tumor differentiation (17-20). However, most studies have focused on the correlation between CSTA expression levels and tumors rather than its inhibitory mechanisms. This study unveiled that CSTA inhibits cellular motility *in vitro* and exerts anti-cancer effects by enhancing the Caspase pathway, indicating potential as a therapeutic target for GC.

This study sought to identify the genes associated with RFS in GC patients using bioinformatics methods and to explore their roles and mechanisms. Our findings provide a theoretical basis for GC research and novel insights into the treatment of GC. We present this article in accordance with the MDAR reporting checklist (available at https://jgo.amegroups.com/article/view/10.21037/jgo-23-941/rc).

Highlight box

Key findings

- Screening out 11 genes highly correlated with recurrence-free survival (RFS) of gastric cancer (GC).
- The strong correlation between genes related to RFS and early differentiated fibroblasts.
- Cystatin A (CSTA) affects the drug sensitivity of GC cells to cisplatin through the caspase pathway.

What is known and what is new?

- CSTA was found downregulated in tumor tissues with metastasis compared with those without metastasis. Overall survival was found with lower CSTA expression.
- Using functional assays, we found that CSTA prevented in vitro apoptosis and motility of GC cells, as well as, the drug sensitivity to cisplatin through the caspase pathway.

What is the implication, and what should change now?

- Our study suggests that the CSTA could be of therapeutic value for inhibiting GC progression. Further research should be conducted, especially on its function in tumor cells or macrophages and its mechanism of action in the tumor microenvironment

Methods

Data sources

Microarray data were retrieved from the Gene Expression Omnibus (GEO; https://www.ncbi.nlm.nih.gov/geo/) database. The GSE54129 data set with transcripts per kilobase of exon model per million mapped reads (TPM) transcriptomic comprises 111 tumor samples from GC patients and 21 normal samples. In addition, RNA-sequencing data and corresponding clinical information for GC were obtained from The Cancer Genome Atlas (TCGA) database (https://portal.gdc.com). The single-cell

sequencing GSE183904 (21) data set was obtained from the GEO database.

Immune checkpoint blockade immunotherapeutic (ICB) cohorts with Fragments Per Kilobase of exon model per Million mapped fragments (FPKM) transcriptomic were collected from the public database [IMvigor210 (2018, anti-programmed cell death 1-ligand 1 (PD-L1), urothelial cancer (22)]. All patients had immune response in the cohort.

DEGs in GSE54129 data set and TCGA

The 'limma' package in R software was used to screen the differentially expressed genes (DEGs) of the GSE54129 and TCGA data sets. Adjusted P values were analyzed to correct for false-positive results. An adjusted P value <0.05 and a log (fold change) >1 for upregulation or a log (fold change) <−1 for downregulation were defined as the screening criteria. Next, a four-set Venn diagram from InteractiVenn (http://www.interactivenn.net/) was used to show the overlapping upregulated and downregulated DEGs. A batch survival analysis was performed on the overlapping genes and genes with significant P values were considered prognostic-related genes. Next, a Venn diagram was used to screen the cross-over genes between the prognostic-related genes and overlapping genes. Subsequently, Gene Ontology (GO) and Kyoto Encyclopedia of Genes and Genomes (KEGG) pathway enrichment analyses of the overlapping genes were performed using the 'clusterProfiler' package. P values were adjusted using the Benjamini-Hochberg method. Adjusted P values <0.05 were considered statistically significant.

Development of a prognostic risk-score model in TCGA cohort

To assess the prognostic value of the 23 overlapping genes, we then conducted a least absolute shrinkage and selection operator (LASSO)-Cox regression analysis to evaluate the association between each gene and survival status in TCGA cohort. The candidate genes were screened and prognostic models were developed using LASSO-Cox regression models (R package "glmnet"). Ultimately, 11 genes and their coefficients were identified, and the penalty parameter (λ) was determined by the minimum criterion. The risk-score formula was expressed as follows:

(0.0402) × C3 + (0.0692) × ESRRG + (0.0544) × CSTA + (0.0623) × CIDEC + (0.1013) × NNMT + (0.1491) × RDH12 + (−0.0805) × CXCL1 + (0.0493) × MFAP2 + (0.0792) × SERPINE1 + (−0.0592) × TP53 + (0.0934) × PSAPL1.

TCGA-GC patients were divided into low- and high-risk subgroups according to the median risk score, and the RFS times of the two subgroups were compared by a Kaplan-Meier analysis. A time-dependent receiver operating characteristic (ROC) curve analysis was performed using the "survivalROC" R package to assess the predictive accuracy of the gene signatures.

Pseudo-time trajectory analysis

To investigate the relationship of the cell pseudo-time trajectories, we performed an analysis of single-cell RNA data using the Monocle R (23) package. To identify the highly variable genes, we applied the following filtering criteria: average expression ≥0.1 and empirical dispersion ≥1× dispersion_fit. Dimensionality reduction was performed using the DDR-tree method. Subsequently, we visualized the results using the "plot_pseudotime_heatmap" function, generating a heatmap.

Cell-cell communication and metabolism analysis

Cellchat (24) R package was used to investigate intercellular communication networks derived from single-cell RNA-sequencing data categorized by distinct cell clusters. SCmetabolism R package (25) was used to assess the activity of the cellular metabolic pathways.

Human GC samples and immunohistochemistry (IHC)

For the IHC analysis, human samples were obtained from the Minhang Hospital affiliated to Fudan University. The study was approved by the Medical Ethics Committee of Minhang Hospital affiliated to Fudan University (protocol code: 2019-38; date of approval: 24 July 2019). The study was conducted in accordance with the Declaration of Helsinki (as revised in 2013). Written informed consent was obtained from the patients.

The samples were incubated overnight at 4 ℃ with anti-CSTA antibody (1:200, Abcam, anti-CSTA antibody, Cat. No. ab128948; Cambridge, UK). The slides were then incubated with HRP-conjugated secondary antibodies for 1 h at room temperature. Subsequently, the slides were visualized using 3,3'-diaminobenzidine for 5 minutes and counterstained with hematoxylin to visualize the nucleus. Finally, images were captured using the Olympus BX51

light microscope (Olympus Corporation).

Cell culture

The GC cell line AGS were obtained from the American Type Culture Collection (ATCC), and the GC cell line SGC-7901 were obtained from the CRL-1740 Lncap. The AGS cell line was cultured in Dulbecco's Modified Eagle Medium (DMEM), while the SGC7901 cell line was cultured in Roswell Park Memorial Institute (RPMI) 1640, along with 10% fetal bovine serum and 1% antibiotics. All the cells were incubated at 37 ℃ with 5% carbon dioxide.

Quantitative real-time-polymerase chain reaction (PCR)

The total RNA was extracted from the test samples using TRIzol® reagent (Invitrogen, USA), and its quality and concentration were assessed with a NanoDrop® 2000 spectrophotometer (Thermo Fisher Scientific, USA). Subsequently, mRNA was reverse-transcribed into cDNA using the PrimeScript™ RT reagent from Takara Bio (Japan). The RNA concentration utilized in the experiment was 1 μg. Following this, FastStart Universal SYBR Green PCR Master Mix Kit (Roche, catalog number 4913914001) was introduced to the sample for conducting RT qPCR to amplify and quantitatively determine the RNA concentration. GAPDH served as an internal control, and gene expression levels were normalized utilizing the $2^{-\Delta\Delta Cq}$ method relative to GAPDH.

The following primers were used: BCL-2 primer: forward: 5'-AGTTCGGTGGGGTCATGTGTG-3', reverse: 5'-CCAGGTATGCACCCAGAGTG-3'; CASP3 primer: forward: 5'-GTAGACGCGTCCAAGTCTCAC TGGCTGTCA-3', reverse: 5'-TCCAGTTTAAACGGAA CTTCTGCGAGGACTTG-3'.

Western blot

Total protein of all samples was harvested using RIPA reagent (Beyotime Institute of Biotechnology), which contains 1 mM PMSF. After measuring the protein concentration using the BCA assay kit (Beyotime Institute of Biotechnology), 40–80% SDS-PAGE was used to separate the proteins in each lane. Protein was then transferred to PVDF membrane (MilliporeSigma). Next, the membrane was incubated overnight at 4 ℃ with primary antibodies against β-Catenin (CTNNB1; #8480, 1:2,000, Cell Signaling Technologies, Inc., BSN, USA), BCL-2 Apoptosis Regulator (BCL2; #15071, 1:1,000, Cell Signaling Technologies, Inc., BSN, USA), Caspase 3 (CASP3; #14420, 1:2,000, Cell Signaling Technologies, Inc.) and CSTA (Cat. No. ab128948, 1:1,000, Abcam). The membrane was washed three times with 0.05% Tween-20 (TBST), and then incubated with HRP coupled second antibody for 1 hour. Finally, an enhanced chemiluminescence detection system (Bio Rad Laboratories, Inc., Hercules, CA, USA) was used to detect protein bands.

Cell Counting Kit 8 (CCK-8) assays

GC cell viability was detected by CCK-8 assays. Briefly, the groups of Control and CSTA-overexpression (CSTA-OE) GC cells were seeded in 96-well plates. After 1, 2, 3, 4 and 5 days, we added 20 μL of CCK-8 buffer to each well at 37 ℃ for 2 hours. Next, we measured the optical density (OD) value at 450 nm on a microplate reader.

Transwell assays

The transwell experiment was divided into the transwell migration experiment and transwell invasion experiment. We seeded 1×10^5 cells suspended in 100 μL of serum-free DMEM into the upper chamber. The lower chamber contained 600 μL of DMEM supplemented with 30% fetal bovine serum. After 8 hours of incubation, the cells were fixed with 4% paraformaldehyde for 30 minutes and stained with crystal violet in water (0.5%). The cells were then viewed under a microscope, and images were taken using the microscope.

Cell apoptosis

Apoptosis in GC cells was assessed using the Annexin-V-APC kit following the manufacturer's protocol. Logarithmic phase cells were plated in 6-well dishes and harvested by trypsinization without EDTA. The collected cells were then suspended in 150 μL of binding buffer, followed by addition of 5 μL of Annexin V staining solution and 10 μL of PI staining solution separately. Subsequently, the cells were pipetted and incubated at room temperature for 15–20 minutes before adding 400 μL of binding buffer to each sample, thoroughly mixed to achieve a final volume of 500 μL for flow cytometry analysis.

Statistical analysis

The data were analyzed using GraphPad Prism 8.0

(GraphPad, Inc., La Jolla, CA, USA) and R (version 4.1.3; R Foundation for Statistical Computing), and the results were expressed as means ± standard deviations (SD). Statistical analyses comprised Student's *t*-test, Wilcoxon rank-sum test, Kruskal-Wallis test, and one-way analysis of variance (ANOVA) to evaluate inter-group differences. Survival curves were constructed employing the Kaplan-Meier method alongside Log-rank testing. The threshold of P<0.05 was employed to denote statistically significant differences between cohorts.

Results

Construction of a prognostic model for GC RFS through gene screening

Following the analysis of TCGA-STAD data, we identified 2,532 genes with upregulated expression and 419 genes with downregulated expression. Subsequent examination of gene expression profiles in GSE54129 revealed 1,124 upregulated genes and 1,239 downregulated genes (*Figure 1A-1C*). The Venn diagram demonstrated an intersection between TCGA-STAD and GSE54129, resulting in a total of 23 GC RFS-related genes (*Figure 1D,1E*). Functional enrichment analysis indicated that these differentially expressed immune regulatory factors primarily participate in pathways associated with the extracellular matrix (ECM), adhesion, and other relevant processes in cancer, suggesting that these pathways could be pivotal factors impacting the prognosis and survival of patients with GC (*Figure 1F,1G*).

The prognostic model of RFS for GC

Using TCGA-STAD data set, a prognostic model for the RFS of GC was constructed. This model incorporated 23 RFS-associated genes and employed a LASSO regression and multivariate Cox analysis. The risk scores were calculated using the following coefficients, including 11 genes (*Figure 2A,2B*):

(0.0402) × C3 + (0.0692) × ESRRG + (0.0544) × CSTA + (0.0623) × CIDEC + (0.1013) × NNMT + (0.1491) × RDH12 + (−0.0805) × CXCL1 + (0.0493) × MFAP2 + (0.0792) × SERPINE1 + (−0.0592) × TP53 + (0.0934) × PSAPL1.

Patients with higher risk scores exhibited a poorer prognosis (*Figure 2C,2D*). The time-dependent area under the curve analysis showed the potential of the 11 GC prognosis-related (GPR) genes prognostic model in predicting RFS among GC patients in TCGA data set (*Figure 2E*). We further winnowed the 23 RFS-related genes down to 11 that were most pertinent to GC prognosis, thereby expediting subsequent analysis and identification of individually clinically applicable genes.

Functional assessment of the prognostic-related genes at the GC single-cell level

In the GSE183904 data set, which comprised 15 GC and 7 adjacent tissue samples, a total of 54,578 cells were clustered, subsequently, these cells could be clustered into 20 subclusters, and clustering and pathway analysis were shown based on the expression of marker genes (Figure S1A,S1B) (21,26,27). The results revealed that subclusters in the GC single-cell atlas were defined as 13 distinct cell subtypes (*Figure 3A*). Through the utilization of five distinct methodologies, we assessed the enrichment scores of the 11 GPR genes across all cellular subpopulations and derived a comprehensive score. The results revealed that GC prognostic-related genes were significantly enriched in the stromal and fibroblast subtypes, further analysis indicates that the proportion of stromal cells in the tumor microenvironment (TME) is significantly higher than in adjacent cancer samples (*Figure 3B,3C*). Further, the gene set variation analysis (GSVA) pathways enrichment highlighted the role of stromal cell types focusing on collagen formation and ECM in the GC TME, which supported our previous findings from the KEGG and GO enrichment analyses (Figure S1C).

The single-cell atlas analysis of GC of functional enrichment and marker gene expression suggests that the stromal cells of interest exhibit similarities to conventional fibroblasts (Figure S2A). This implies that these stromal cells may represent a subtype of fibroblasts undergoing early-stage differentiation. The enrichment score of GPR genes in stromal cells surpasses that observed in other GC-TME cell subtypes (*Figure 3D*, Figure S2B). Additionally, validation through pseudo-time analysis confirmed that these stromal cells were indeed in an early stage of differentiation. Our previous analysis also indicated that this early fibroblast subtype was predominantly clustered in cancer tissues, with only a small proportion found in adjacent tissues, indicating active expansion within GC. The temporal expression patterns of the 11 GPR genes further suggested their involvement in regulating differentiation and maturation functions at different stages within these three fibroblast subpopulations (*Figure 3E*, Figure S2C).

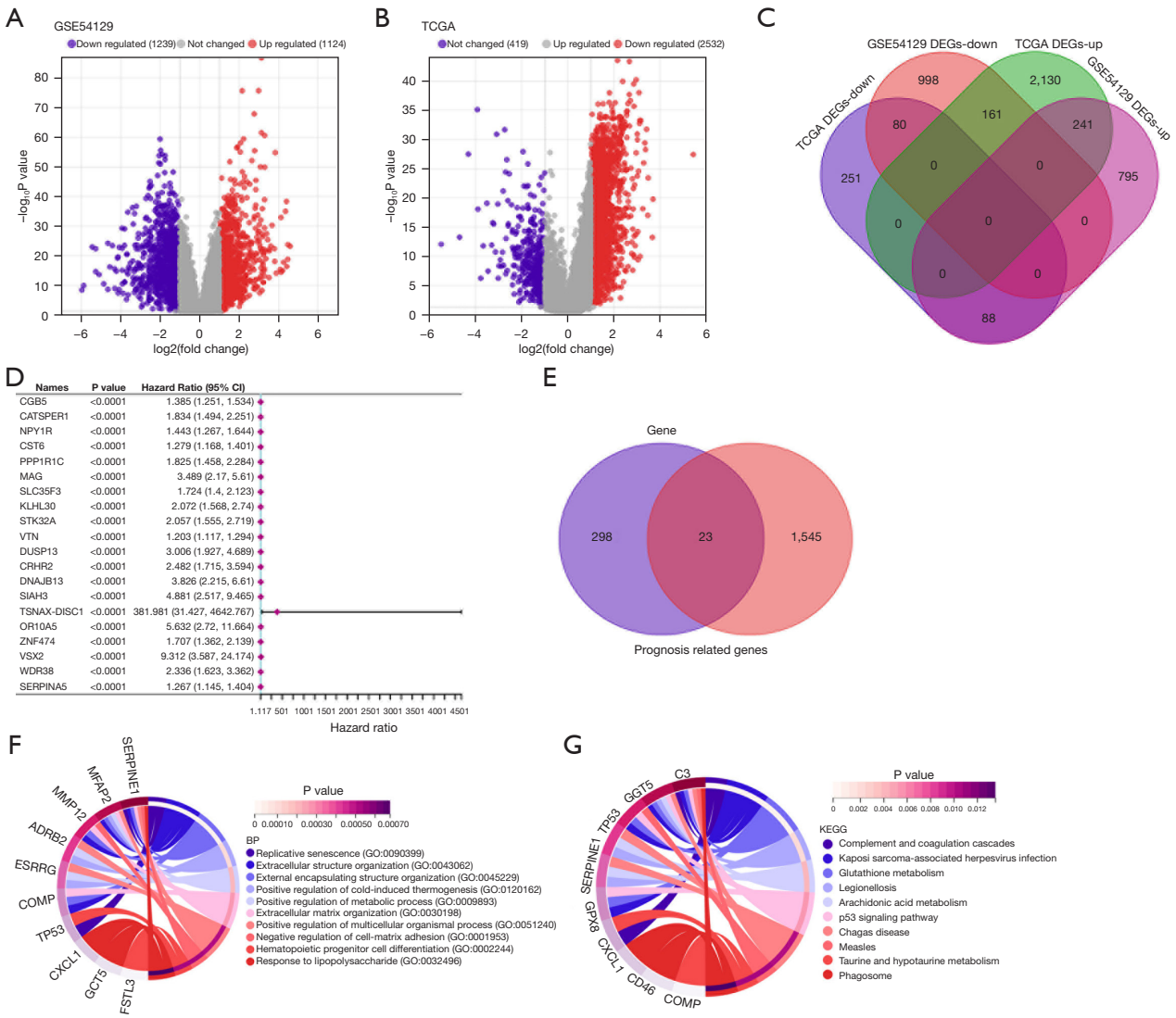

Figure 1 Identification and construction of prognostic models based on Recurrence-free survival-related genes. (A,B) DEGs between the tumor tissues and adjacent tissues in the GC. The red dots represent significantly up-regulated, the blue dots represent significantly down-regulated, and the gray dots represent no difference change. (A) DEGs in GSE54129. (B) DEGs in the TCGA-STAD data set. (C) Intersection of DEGs between GSE54129 and TCGA data set. (D) Top 20 prognostic genes in TCGA-STAD based on the entire gene set. (E) Venn diagram showing the intersection between the genes from GSE54129 and TCGA-STAD and prognostic genes. (F) GO-BP enrichment analysis of the 23 overlapping genes. (G) KEGG enrichment analysis of the 23 overlapping genes. TCGA, the Cancer Genome Atlas; DEGs, differentially expressed genes; CI, confidence interval; BP, biological process; GO, Gene Ontology; KEGG, Kyoto Encyclopedia of Genes and Genomes; GC, gastric cancer; STAD, stomach adenocarcinoma.

Cancer-associated fibroblasts (CAFs) are crucial components of the TME, and based on specific molecular characteristics (28,29), they can be classified into the following subtypes: myofibroblastic CAFs (pan-myCAFs), proliferative fibroblastic CAFs (pan-dCAFs), inflammatory fibroblastic CAFs (pan-iCAFs), and normal fibroblastic CAFs (pan-pCAFs). We divided the stromal cell subgroups into high and low score groups, and found that, apart from the pan-myCAFs subtype, the other subtypes were highly associated with stromal cells (*Figure 3F*). Using "scMetabolism" to assess the activation levels of KEGG metabolic pathways of two stromal cells subgroups, the results showed that cells

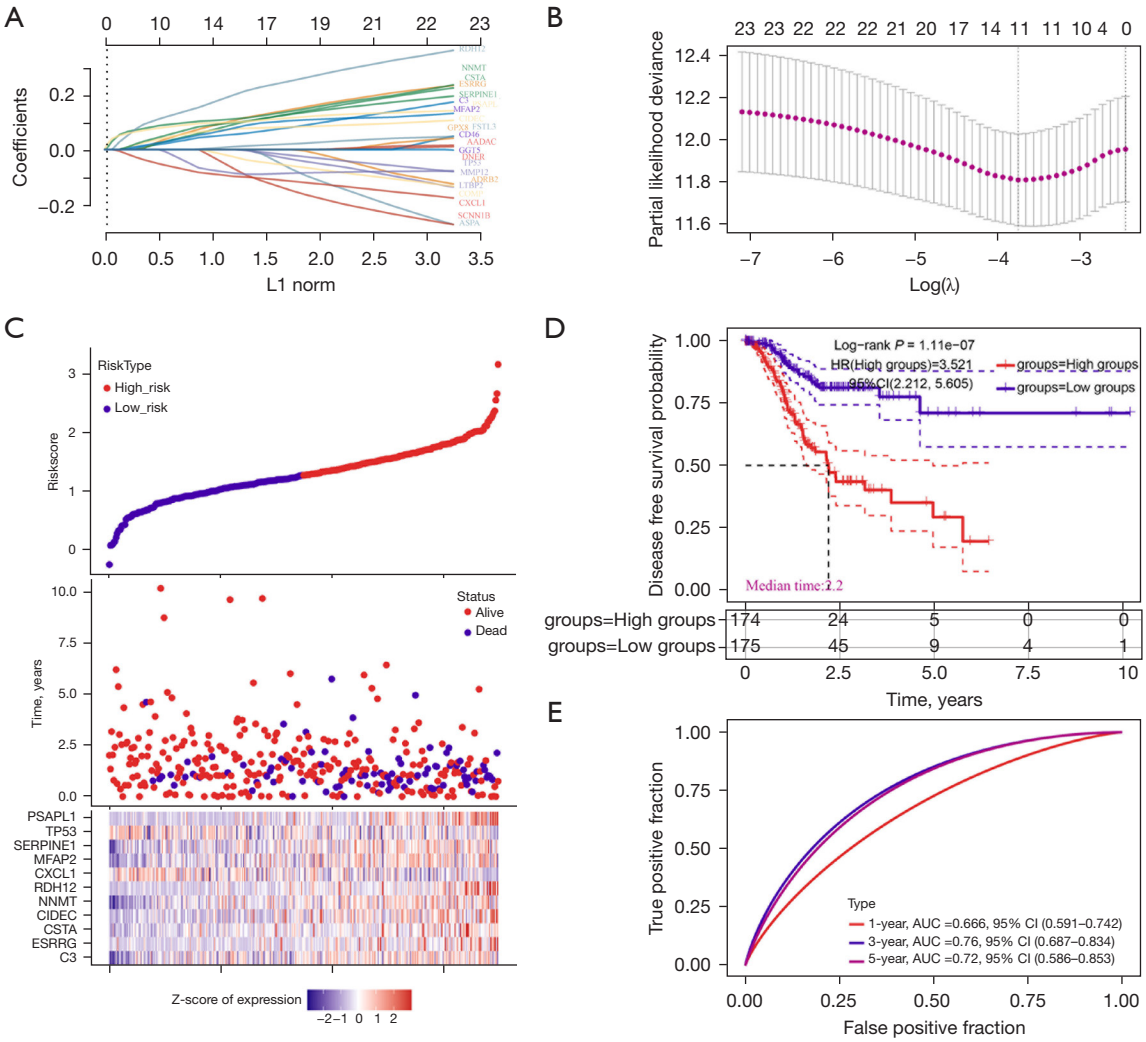

Figure 2 Construction of a prognostic model related to recurrence-free survival. (A,B) LASSO regression with tenfold cross-validation of 23 genes. (C) Survival of GC patients by the Signature risk score. (D) RFS probability analysis of Kaplan-Meier analysis of high-risk group and low-risk group. (E) ROC curves for predicting 1-, 3-, and 5-year survival in the risk model. HR, hazard ratio; CI, confidence interval; AUC, area under the curve; LASSO, least absolute shrinkage and selection operator; GC, gastric cancer; RFS, recurrence-free survival; ROC, receiver operating characteristic.

in the score_high subgroup had higher metabolic levels (Figure S2D). The cell-cell communication reveals that the score_high subgroup cells exhibited enhanced communication with various subgroups in the intratumoral environment, particularly endothelial cells (ECs). They showed enhanced communication with various T cells through GZMA-F2R ligand-receptor interactions (*Figure 4A,4B*). The enhanced crosstalk with ECs and T cells may have a potential impact on the TME, thereby influencing patient RFS. Furthermore, by analyzing the DEGs between the groups and conducting a GO pathway enrichment analysis, we identified 15 upregulated genes enriched in the peptide metabolism, hypoxia, and ECM formation pathways in the high score subgroup compared to the low score subgroup. Additionally, 69 downregulated genes were enriched in the RNA splicing pathways (Figure S2E,S2F). Additionally, the pseudo-time analysis revealed that stromal cells within the high score subgroup tended to demonstrate a more differentiated state (*Figure 4C*).

To further investigate the effect of the top 30 gene signatures of stromal cells on patient survival after

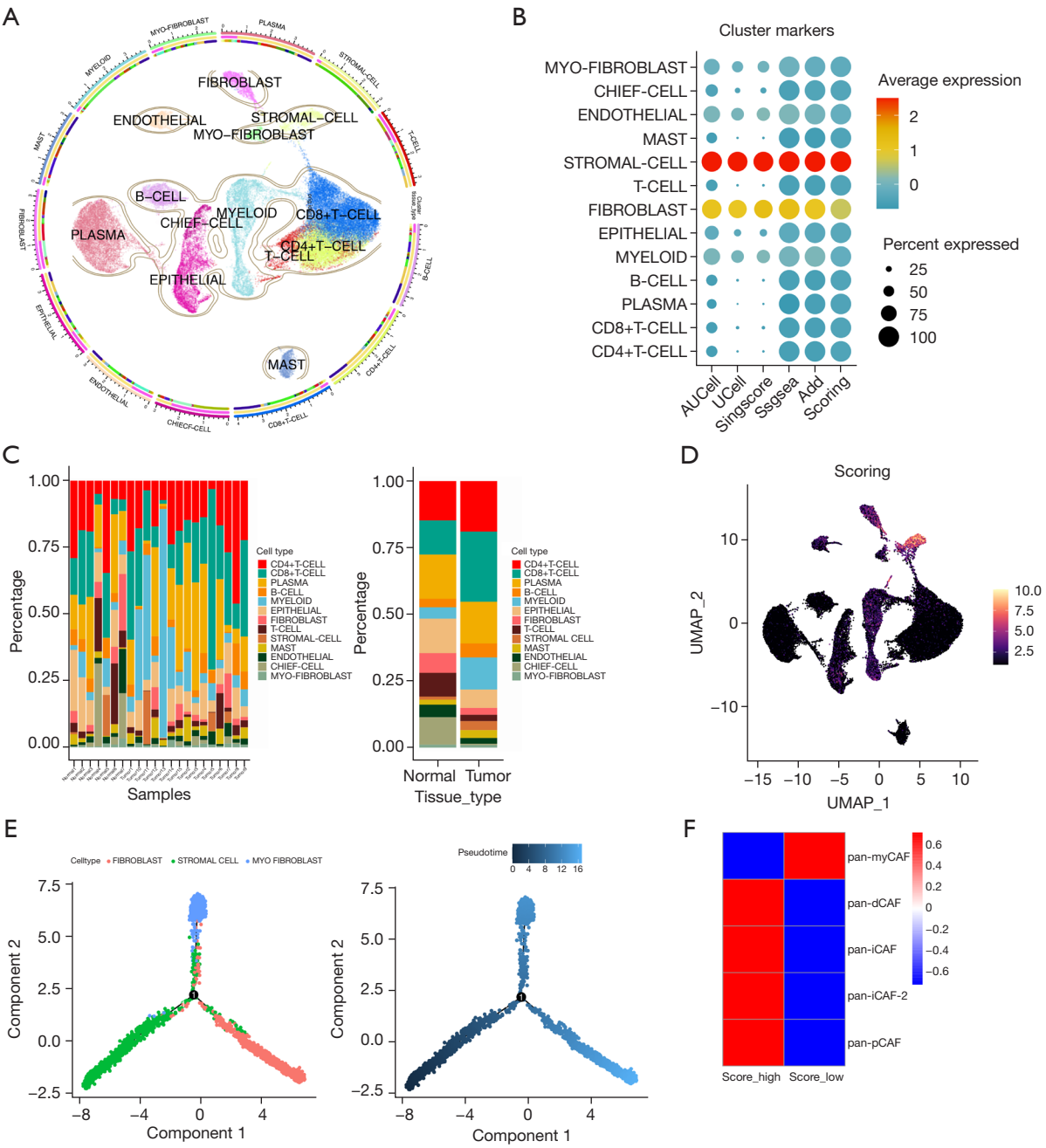

Figure 3 The landscape of GC prognostic-related gene scores in *tumor* microenvironment cells in gastric cancer. (A) UMAP diagram illustrates the clustering outcomes of the 13 cell types obtained from normal and GC tissues, with distinct colors representing individual cell types. (B) A heatmap demonstrates the expression score of marker genes in specific cellular subpopulations based on enrichment analysis using four methods including AUCell, UCell, ssgsea, Add, then integrate the scores obtained from the aforementioned method to create a new composite score, which labeled as 'scoring'. (C) A stacked histogram depicting the proportion of 13 main cell subtypes in total cells derived from normal and cancerous stomach tissues. Histogram depicting the proportion of three main cell types in normal and cancerous stomach tissues. (D) The UMAP show the GPR genes score in distinct cell subtypes. (E) A pseudo-time analysis was performed to investigate the differentiation trajectories of three types of stromal cells and the temporal expression patterns of 11 GPR genes. (F) A heatmap illustrating the relationships between stromal cells grouped by various scores and different CAF subtypes. UMAP, The Uniform Manifold Approximation and Projection for Dimension Reduction; GC, gastric cancer; Add, addmodule score; GPR, GC prognostic-related.

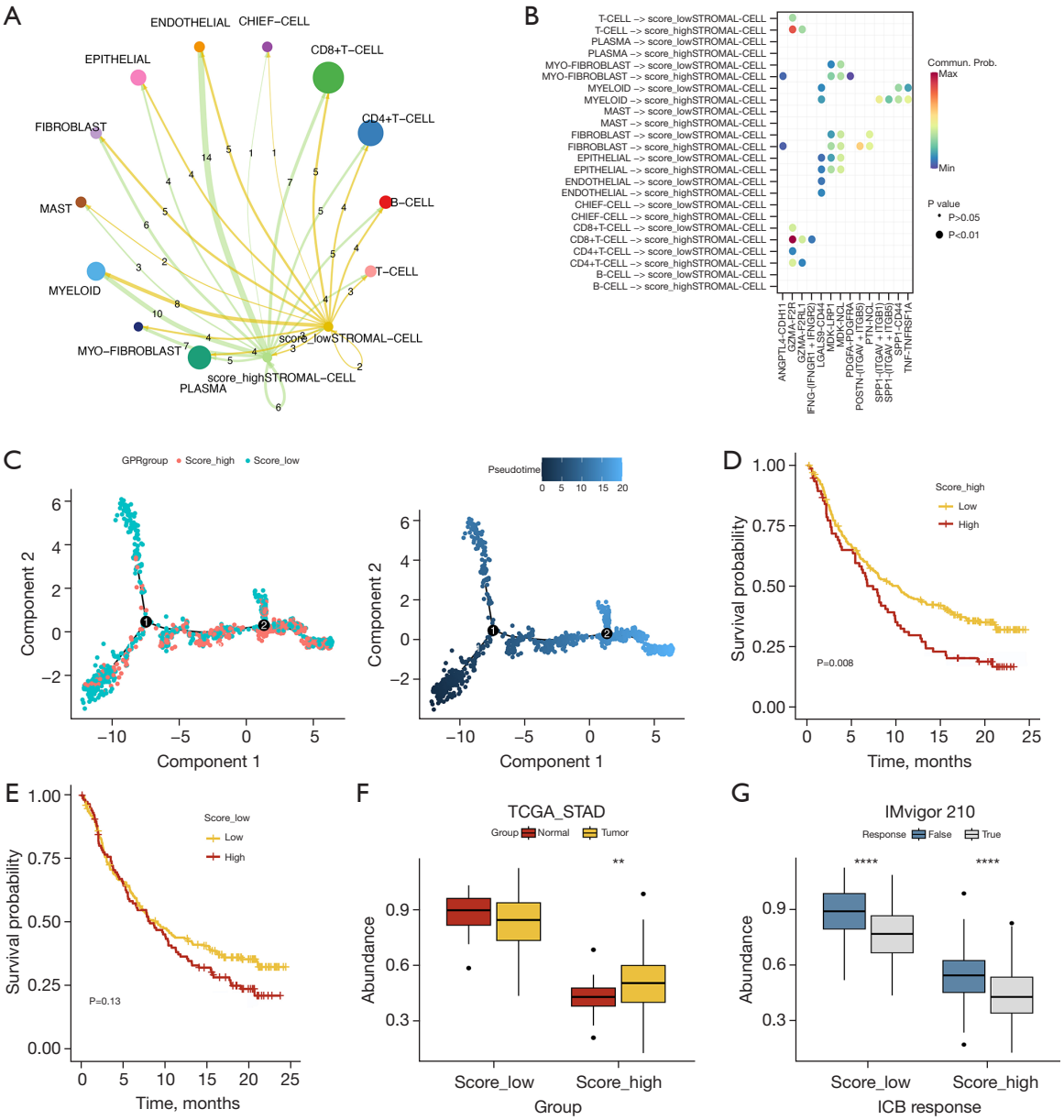

Figure 4 Functional evaluation of prognosis-related genes at the single-cell level. (A) The cell-cell communication analysis revealed the differences in the communication strength between the stromal cells and GC-TME cells across the different score groups. (B) A heatmap showing the differences in the communication strength of the receptor-ligand pathways between the stromal cells and GC-TME cells across different score groups. (C) A pseudo-time analysis was used to trace the differentiation trajectory of stromal cells across different score groups. (D) The Kaplan-Meier curves demonstrated the impact of the top 30 marker genes in score_high group stromal cells on the prognosis of the IMvigor 210 immunotherapy cohort. (E) The Kaplan-Meier curves demonstrated the impact of the top 30 marker genes in score_low group stromal cells on the prognosis of the IMvigor 210 immunotherapy cohort. (F,G) The box plot demonstrates the difference in expression scores of the top 30 marker genes in score_low and score_high cells across cohorts (**, P<0.01; ****, P<0.0001). (F) Differential expression scores between cancerous and para-cancerous tissues in TCGA-STAD cohort. (G) Differences in the expression scores between the treatment response (True) and non-response (False) samples were observed in the IMvigor 210 (prostate cancer immunotherapy cohort). GPR, GC prognostic-related; UMAP, The Uniform Manifold Approximation and Projection for Dimension Reduction; TCGA, the Cancer Genome Atlas; STAD, Stomach adenocarcinoma; ICB, immune checkpoint blockade; GC, gastric cancer; TME, tumor microenvironment.

treatment, we used the IMvigor 210 immunotherapy and TCGA-STAD cohort. The results revealed that in the IMvigor 210 cohort, the top 30 gene signatures of the score_high stromal cell subset had a significant effect on patient survival after treatment, with the low-expression group showing higher survival rates (*Figure 4D*,*4E*). In TCGA-STAD cohort, the top 30 gene signatures of the score_high stromal cells were significantly more upregulated in the tumor tissues (*Figure 4F*). In IMvigor 210 cohort, the top 30 gene signatures of the score_high stromal cells were significantly more downregulated in treatment response group (*Figure 4G*).

In summary, our assessment of the 11 GPR genes revealed their predominant enrichment in an early fibroblastic stromal cell population. The high-scoring stromal cells exhibited increased activity in various pathways related to metabolism, differentiation, and communication. Additionally, the upregulated genes in the score_high stromal cells were enriched in pathways associated with peptide metabolism and hypoxia, suggesting a potential link to hypoxia-induced processes. Moreover, the signature of these score_high stromal cells had an impact on patient survival after treatment within the bulk cohort. This single-cell analysis provides a theoretical basis for the clinical application of the prognostic model developed earlier in this study.

CSTA inhibits the tumor malignant phenotype of GC cells

The role and mechanism of CSTA in GC remained unclear among the 11 genes. By further sub-grouping the epithelial cell subpopulation into tumor cells and normal cells (*Figure 5A*,*5B*). In comparison to normal epithelial cells, the expression of CSTA was elevated in cancerous epithelium (*Figure 5C*,*5D*). The IHC results revealed that CSTA was lowly expressed in cancer tissues (*Figure 5E*). The Western blot showed the expression levels of CSTA in various GC cell lines. The results demonstrated that CSTA was more highly expressed in the normal tissue groups and multiple GC cell lines, particularly in AGS, SGC-7901, and HGC-27 (*Figure 5F*). The TCGA-STAD data are consistent with our above research results (*Figure 5G*).

Further, we overexpressed CSTA in the AGS and SGC-7901 cells, designated as CSTA overexpression (CSTA-OE) (*Figure 6A*,*6B*). Using CCK-8, transwell assays, colony formation and scratch assays revealed that the overexpression of CSTA significantly suppressed the migration and invasion of the GC cells (*Figure 6C-6K*).

CSTA facilitates GC cell apoptosis by activating the caspase-dependent pathway

Flow cytometry was employed to assess the effect of CSTA-OE on apoptosis in the GC cells. The results revealed a significant alteration in the apoptotic ratio of the AGS and SGC-7901 cells with CSTA-OE compared to the control group (*Figure 7A*,*7B*). Further, we investigated the effects of CSTA-OE on pro-apoptotic and anti-apoptotic proteins. Caspase 3, the ultimate executor of the caspase-dependent apoptotic pathway, and apoptosis regulator BCL-2, a classic protein in the anti-apoptotic pathway, were selected as the targets of our study. The results demonstrated that Caspase 3 expression was upregulated and BCL-2 expression was downregulated in response to CSTA-OE; similar results were observed at the messenger RNA level (*Figure 7C-7E*).

Caspase 3, a key protein and the final executor of the caspase-dependent apoptotic pathway, exerts pro-apoptotic effects by cleaving to downstream cell survival-related proteins. The GSEA pathway analysis revealed a negative correlation between CSTA expression and the Wnt pathway. Therefore, we examined the expression levels of β-catenin, a core protein in the Wnt pathway, in both groups. Interestingly, we observed a decrease in β-catenin expression in the CSTA-OE group, which suggests that CSTA may induce the degradation of β-catenin through the caspase pathway, thereby exerting its inhibitory effects on the malignant phenotype of GC (*Figure 7F-7H*).

The overexpression of CSTA enhances the apoptotic effect of cisplatin

Combination therapy involving cisplatin and other agents remains a frontline approach in GC treatment, as combining multiple drugs can overcome resistance issues and reduce toxic side effects.

The experimental groups were divided into four categories: the PCDH group (NC), the CSTA-OE group, the PCDH group treated with 5 μM of cisplatin (cis) for 48 hours, and the CSTA-OE group treated with 5 μM of cisplatin for 48 hours (cis + CSTA-OE). The levels of proliferation, migration, invasion, and colony formation among the four groups were assessed using CCK-8, transwell, and colony formation assays. The results demonstrated that CSTA-OE enhanced the tumor-killing ability of cisplatin in the GC cells (*Figure 8A-8D*). The results of flow cytometry showed that the addition of cis + CSTA-OE increased the level of cell apoptosis in the group

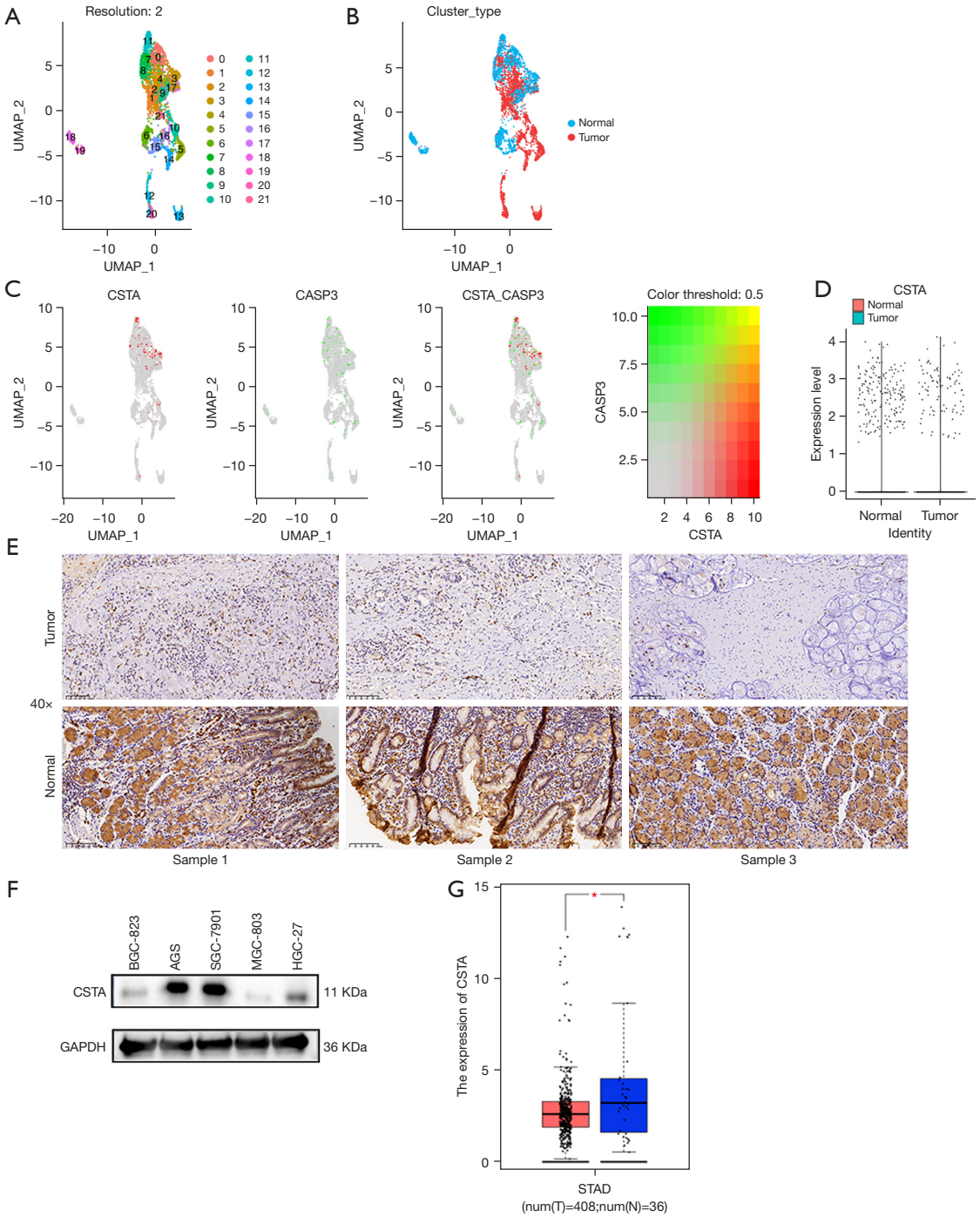

Figure 5 Localization of CSTA in the TME of gastric cancer. (A) UMAP diagram showing the regrouping of epithelial cell subsets. (B) The UMAP reveals the distinction between cancer epithelium and normal tissue epithelium of the GC single-cell atlas. (C) The UMAP reveals the localization of CSTA and CASP3 in the epithelial cell subsets. (D) An organogram showing the expression levels of CSTA in solitary neoplastic cells and the normal epithelial subpopulation. (E) IHC staining results of CSTA in GC and normal tissue (×40-fold). (F) Protein expression levels of CSTA in GC cell lines detected by Western blot. (G) The box plot shows the difference of expression levels of CSTA in TCGA database, the red box represent the tumor group (T), the blue box represent the normal group (N) (*, P<0.05). UMAP, The Uniform Manifold Approximation and Projection for Dimension Reduction; CSTA, Cystatin A; CASP3, Caspase 3 gene name; STAD, stomach adenocarcinoma; TME, tumor microenvironment; GC, gastric cancer; IHC, immunohistochemistry; TCGA, the Cancer Genome Atlas.

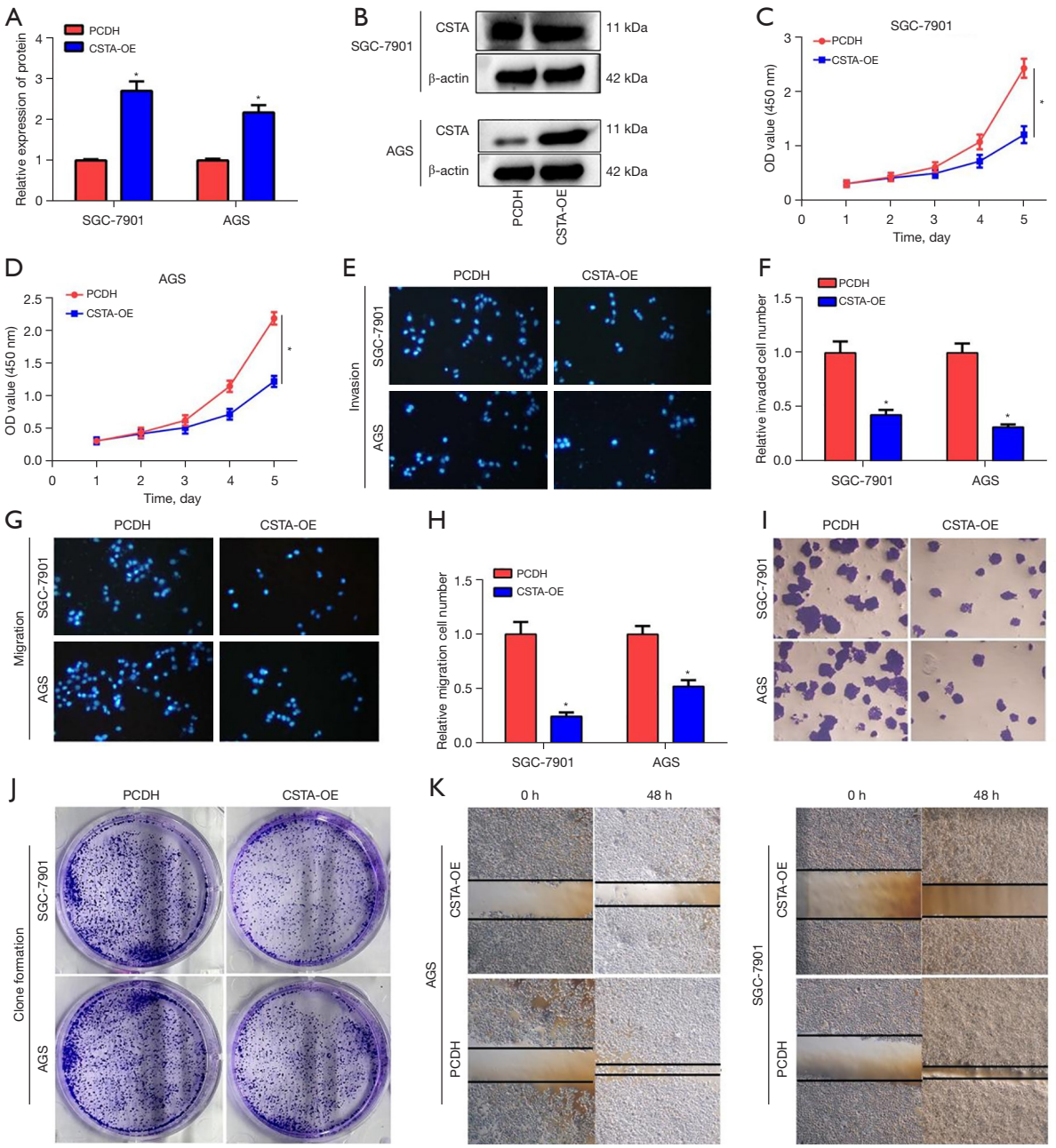

Figure 6 The overexpression of CSTA significantly inhibits the malignant phenotype of gastric cancer cells. (A,B) Protein expression analysis of CSTA-OE and control group (PCDH) in GC cell lines SGC-7901 and AGS. (A) The histogram presents the quantitative analysis of CSTA protein expression between the groups using Image J (*, P<0.05). (B) Western blot analysis of CSTA-OE in GC cell lines. (C,D) The line plots presents CCK-8 assays were used to assess the SGC-7901 and AGS cells proliferation activity between CSTA-OE and PCDH groups (*, P<0.05). (E-H) Transwell assays were used to assess the cell invasion and migration ability between the groups, through staining with DAPI further microscopy (200× magnification). The histogram present quantitative analysis by using Image J (*, P<0.05). (I) Colony formation assays were used to assess the cell clonogenicity between the CSTA-OE and PCDH groups, through staining with 0.1% crystal violet further microscopy (400× magnification). (J) Colony formation assays were used to assess the cell clonogenicity between the CSTA-OE and PCDH groups through staining with 0.1% crystal violet in six-well plates (the diameter is 85 mm). (K) Scratch assays were used to assess the cell migration ability between the experimental and control groups (200× magnification). PCDH, pCDH Plasmid vector control; CSTA, cystatin A; OE, overexpression; OD, optical density; GC, gastric cancer; CCK8, Cell Counting Kit-8; DAPI, 4',6-diamidino-2-phenylindole.

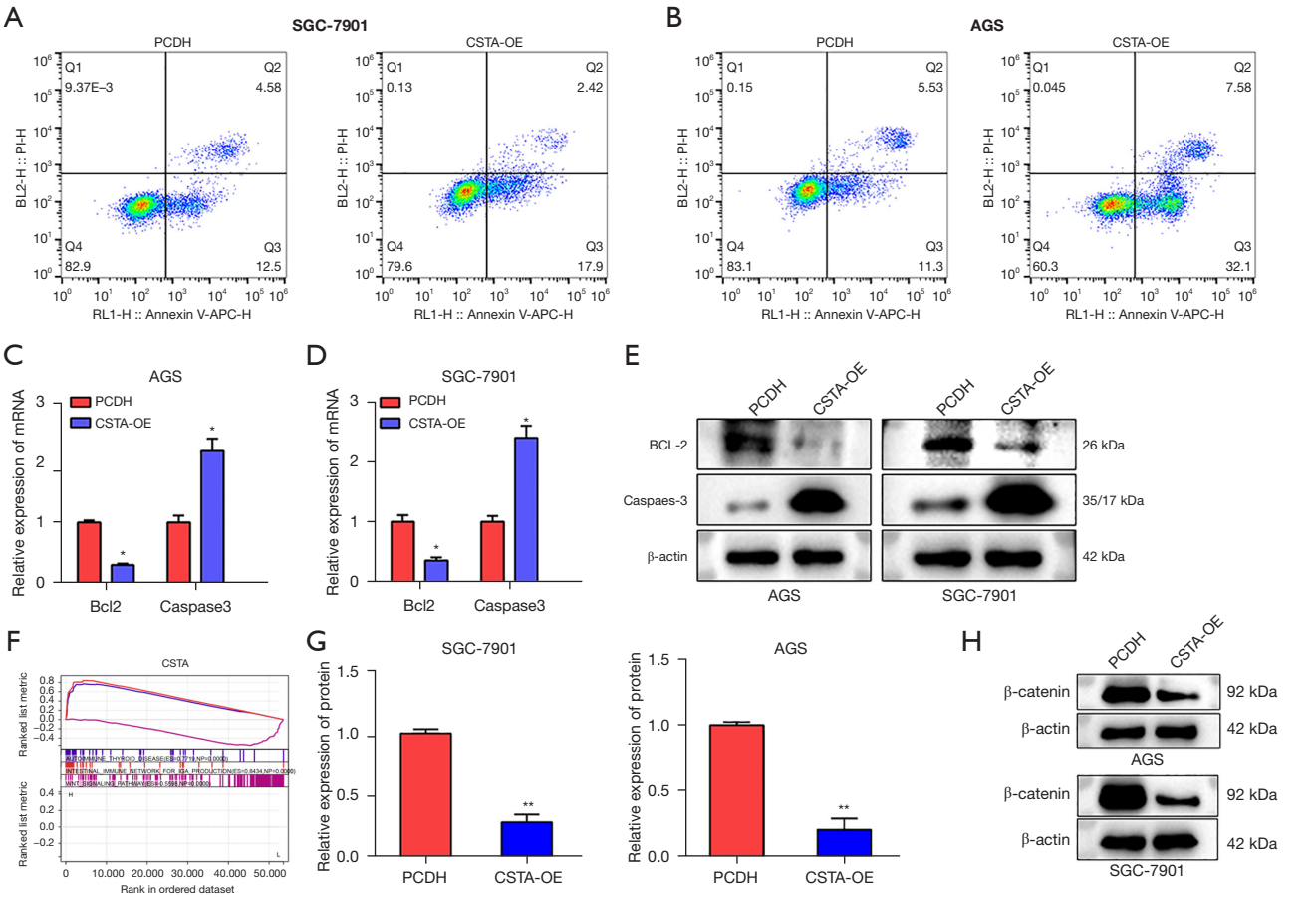

Figure 7 CSTA facilitates the inhibition of gastric cancer cells through the caspase apoptotic pathway. (A,B) Flow cytometry was used to compare the apoptotic levels between the CSTA-OE and control group (PCDH) in GC cell lines SGC-7901 and AGS. (C,D) The bar chart show mRNA expression levels of Caspase-3 and the anti-apoptotic protein BCL-2 were compared between CSTA-OE and PCDH groups in gastric cancer cell lines AGS and SGC-7901 using qRT-PCR (*, P<0.05). (E) The expression of apoptosis-related proteins Caspase 3 and anti-apoptotic protein BCL-2 was detected by western blot. (F) A GSEA was conducted to examine the biological pathway of CSTA in GC. (G) Protein expression analysis of CSTA-OE and PCDH group GC cell lines SGC-7901 and AGS. The histogram presents the quantitative analysis of β-catenin protein expression of SGC-7901 and AGS between the groups using Image J (**, P<0.01). (H) The difference expression of β-catenin of the group was detected by western blot. PCDH, pCDH Plasmid vector control; CSTA, Cystatin A; OE, overexpression; PI, propidium iodide; APC, allophycocyanin; GSEA, gene set enrichment analysis; GC, gastric cancer; qRT-PCR, quantitative real-time polymerase chain reaction.

remarkably (*Figure 8E*).

CSTA-OE also increased the sensitivity of the GC cells to cisplatin (Figure S3A). The expression levels of the pro-apoptotic protein Caspase 3 and the anti-apoptotic protein BCL-2 were measured among the four groups. The results showed that CSTA-OE combined with cisplatin significantly increased the expression of Caspase 3 and suppressed the expression of BCL-2 (Figure S3B).

Discussion

GC is one of the most prevalent cancers worldwide, with a high incidence rate in many countries, particularly in Asia (30). Chemotherapy remains the frontline treatment for locally unresectable and metastatic stomach cancer. However, this treatment option has inherent drawbacks, such as a lack of specificity, severe side effects, and tumor resistance (3). Thus, we sought to identify novel potential

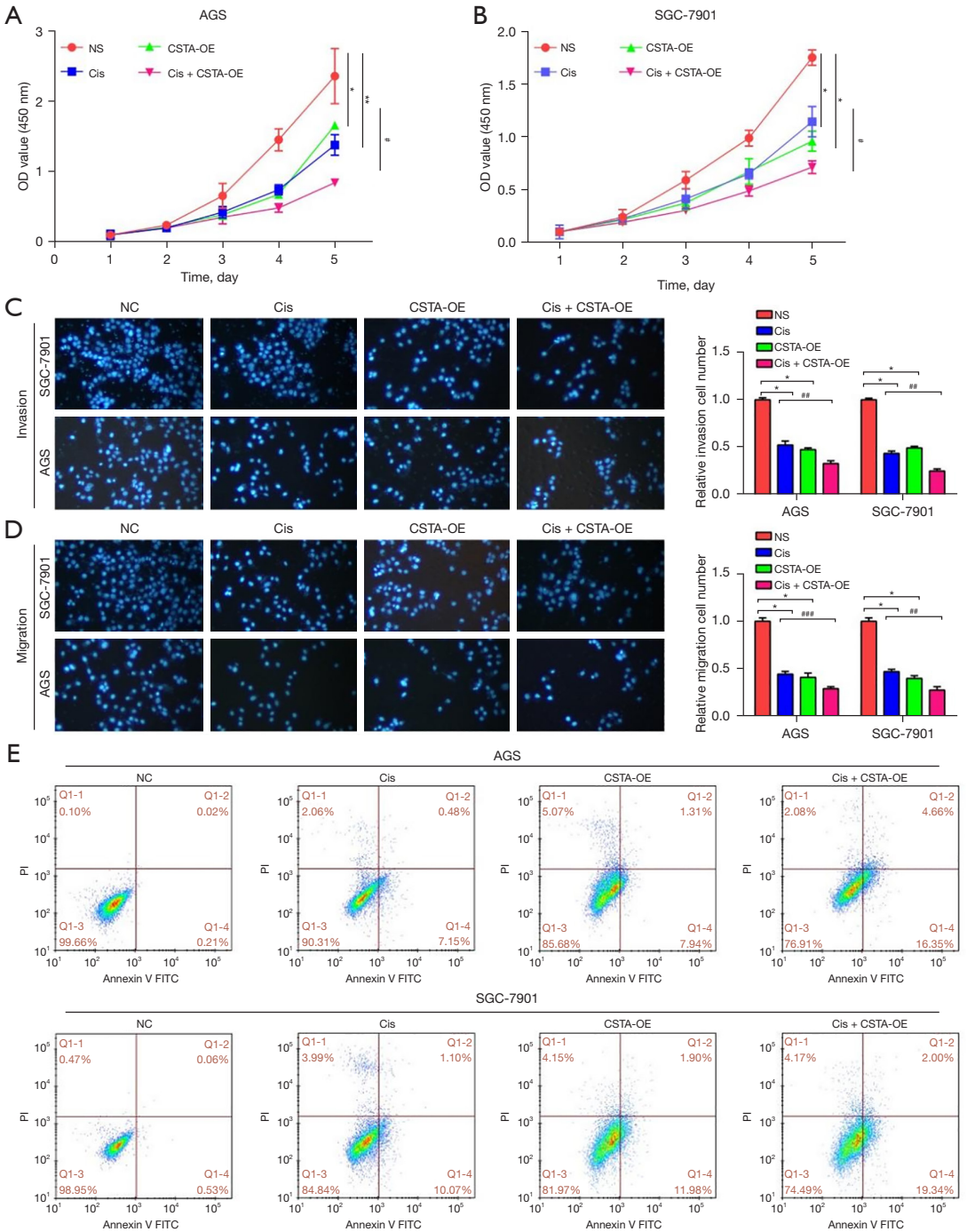

Figure 8 CSTA-overexpression enhances the pro-apoptotic effect of cisplatin. (A,B) Line plots depict the proliferative activity assessed using the CCK-8 method in AGS and SGC-7901 cell lines across various experimental groups (NS:PCDH, CSTA-OE:CSTA-overexpression. Cis: cisplatin add PCDH, Cis + CSTA-OE: cisplatin add CSTA-OE) (*, P<0.05; **, P<0.01; #, P<0.05). (C,D) Transwell assays were used to assess the migration and invasion abilities of the GC cells among the four experimental groups, through staining with DAPI further microscopy (200× magnification). And the histogram present quantitative analysis by using Image J (*, P<0.05; ##, P<0.01; ###, P<0.001). (E) A flow cytometry analysis was conducted to quantify the variance in apoptotic levels of gastric cancer cells across the four experimental groups. OD, optical density; NS, no statistical difference; Cis, cisplatin; CSTA, Cystatin A; OE, overexpression; PI, propidium iodide; FITC, fluorescein isothiocyanate; pCDH Plasmid vector control; GC, gastric cancer; DAPI, 4',6-diamidino-2-phenylindole.

targets in stomach cancer using bioinformatics approaches.

Firstly, using a bioinformatics analysis, the construction of a prognostic model to predict RFS in patients with GC was undertaken, furthermore, we identified 11 pivotal GC RFS-associated genes (i.e., *C3*, *ESRRG*, *CSTA*, *CIDEC*, *NNMT*, *RDH12*, *CXCL1*, *MFAP2*, *SERPINE1*, *TP53*, and *PSAPL1*) and explored their potential functions using the GC single-cell cohort. The findings indicate that an early fibroblast-like stromal cell population may serve as a crucial determinant of GC RFS (31). This population predominantly resides in tumor tissue and possesses the potential to differentiate into mature fibroblasts and myofibroblasts (32).

Numerous studies have unequivocally demonstrated the pivotal role of immune evasion in the initiation and progression of cancer, particularly in GC where CAFs impede immune cell infiltration through paracrine or direct mechanisms, thereby diminishing the immune system's capacity to recognize and eliminate cancer cells, consequently fostering the onset and advancement of GC (33). CAFs also secrete a myriad of cytokines to induce T cell infiltration, proliferation, differentiation, and apoptosis, thus detrimentally affecting normal T cell immune function (34). Furthermore, CAFs are proficient at remodeling the ECM, establishing a physical barrier that obstructs T lymphocyte infiltration and contributes to tumor immune evasion (35). Additionally, CAF secreted miR-522 suppresses ferroptosis and promotes acquired chemo-resistance in GC (36). The hypoxic conditions within the TME can also stimulate GC CAFs to release vascular endothelial growth factor (VEGF) in order to enhance tumor angiogenesis (37,38).

The expression scores of RFS-associated genes in stromal cells are correlated with their differentiation statuses and the distinct expression patterns of CAF marker genes. Stromal cells with high scores are likely to communicate with various cells, including ECs and T cells, via multiple receptor-ligand pathways, thereby influencing tumor progression. The gene signatures of these cells could serve as prognostic indicators for patient treatment outcomes.

Consequently, our prognostic model and gene set, based on RFS-associated genes, could be employed to assess the activation level of early fibroblasts in the microenvironment of GC patients, offering novel insights into the exploring the mechanism of GC occurrence and progression. The primary obstacle in therapeutic interventions for GC resides in the formidable resistance to traditional chemotherapeutic agents (e.g., cisplatin) and suboptimal response rates to innovative drug modalities (e.g., targeted therapy and immunotherapy) (2). Therefore, our prognostic model and the 11 identified genes hold substantial promise, potentially serving as therapeutic targets that could impede disease progression and augment patient survival, this study provides new evidence of the clinical utility of prognostic genes, and establishes a theoretical foundation and scientific basis for the study and treatment of CSTA in stomach cancer.

CSTA (39), also known as cystatin or acidic cysteine proteinase inhibitor, belongs to the type I or stefin subgroup of known cysteine protease inhibitors. It is an 11-kDa single-chain intracellular cysteine proteinase inhibitor that can inhibit papain, cathepsins B/H/L, and cysteine proteinase activities (40). This study was the first to demonstrate the role of CSTA in stomach cancer. Specifically, this study showed that CSTA is lowly expressed in cancer tissue samples, and exerts anticancer effects by promoting the expression of apoptotic proteins and enhancing the sensitivity of stomach cancer cells to cisplatin.

Conclusions

In conclusion, through the development of a prognostic model for RFS in GC patients, we have successfully pinpointed 11 genes with potential clinical significance. These genes, predominantly enriched in early-stage stromal cells, can indirectly anticipate the abundance of early-stage fibroblasts in cancer tissue and consequently forecast the prognosis of GC patients. Despite the study's demonstration of CSTA's antitumor effect through the enhancement of the Caspase-dependent apoptotic pathway in GC cells, further exploration is needed to elucidate the mechanisms of CSTA-mediated tumor inhibition, its specific role in the stomach cancer microenvironment, particularly in macrophages, and its value as a novel target. It should be noted that our exploratory study is limited by the limited profundity of scRNA-sequencing data and the small sample size. The results also need additional validation in more patients.

Acknowledgments

Funding: This work was supported by a subaward from the National Science Foundation of China (No. 8217100675).

Footnote

Reporting Checklist: The authors have completed the MDAR

reporting checklist. Available at https://jgo.amegroups.com/article/view/10.21037/jgo-23-941/rc

Data Sharing Statement: Available at https://jgo.amegroups.com/article/view/10.21037/jgo-23-941/dss

Peer Review File: Available at https://jgo.amegroups.com/article/view/10.21037/jgo-23-941/prf

Conflicts of Interest: All authors have completed the ICMJE uniform disclosure form (available at https://jgo.amegroups.com/article/view/10.21037/jgo-23-941/coif). All authors report that this work was supported by National Science Foundation of China (No. 8217100675) subaward. The authors have no other conflicts of interest to declare.

Ethical Statement: The authors are accountable for all aspects of the work in ensuring that questions related to the accuracy or integrity of any part of the work are appropriately investigated and resolved. The study was conducted in accordance with the Declaration of Helsinki and was approved by the Medical Ethics Committee of Minhang Hospital affiliated to Fudan University (protocol code: 2019-38; date of approval: 24 July 2019). Written informed consent was obtained from the patients.

References

1. Decourtye-Espiard L, Guilford P. Hereditary Diffuse Gastric Cancer. Gastroenterology 2023;164:719-35.
2. Guan WL, He Y, Xu RH. Gastric cancer treatment: recent progress and future perspectives. J Hematol Oncol 2023;16:57.
3. Choi IJ, Kim CG, Lee JY, et al. Family History of Gastric Cancer and Helicobacter pylori Treatment. N Engl J Med 2020;382:427-36.
4. Arnold M, Park JY, Camargo MC, et al. Is gastric cancer becoming a rare disease? A global assessment of predicted incidence trends to 2035. Gut 2020;69:823-9.
5. Lordick F. Chemotherapy for resectable microsatellite instability-high gastric cancer? Lancet Oncol 2020;21:203.
6. Thrift AP, Wenker TN, El-Serag HB. Global burden of gastric cancer: epidemiological trends, risk factors, screening and prevention. Nat Rev Clin Oncol 2023;20:338-49.
7. Murad AM, Santiago FF, Petroianu A, et al. Modified therapy with 5-fluorouracil, doxorubicin, and methotrexate in advanced gastric cancer. Cancer 1993;72:37-41.
8. Ajani JA, D'Amico TA, Almhanna K, et al. Gastric Cancer, Version 3.2016, NCCN Clinical Practice Guidelines in Oncology. J Natl Compr Canc Netw 2016;14:1286-312.
9. Van Cutsem E, Bang YJ, Feng-Yi F, et al. HER2 screening data from ToGA: targeting HER2 in gastric and gastroesophageal junction cancer. Gastric Cancer 2015;18:476-84.
10. Fuchs CS, Doi T, Jang RW, et al. Safety and Efficacy of Pembrolizumab Monotherapy in Patients With Previously Treated Advanced Gastric and Gastroesophageal Junction Cancer: Phase 2 Clinical KEYNOTE-059 Trial. JAMA Oncol 2018;4:e180013.
11. Tabernero J, Van Cutsem E, Bang YJ, et al. Pembrolizumab with or without chemotherapy versus chemotherapy for advanced gastric or gastroesophageal junction (G/GEJ) adenocarcinoma: The phase III KEYNOTE-062 study. American Society of Clinical Oncology 2019. Available online: https://doi.org/10.1200/JCO.2019.37.18_suppl.LBA4007
12. Jun JK, Choi KS, Lee HY, et al. Effectiveness of the Korean National Cancer Screening Program in Reducing Gastric Cancer Mortality. Gastroenterology 2017;152:1319-1328.e7.
13. Japanese gastric cancer treatment guidelines 2014 (ver. 4). Gastric Cancer 2017;20:1-19.
14. Yuan L, Hu C, Yu P, et al. High HDAC5 expression correlates with a poor prognosis and the tumor immune microenvironment in gastric cancer. Ann Transl Med 2022;10:990.
15. Takahashi H, Asano K, Kinouchi M, et al. Structure and transcriptional regulation of the human cystatin A gene. The 12-O-tetradecanoylphorbol-13-acetate (TPA) responsive element-2 site (-272 to -278) on cystatin A gene is critical for TPA-dependent regulation. J Biol Chem 1998;273:17375-80.
16. Gupta A, Nitoiu D, Brennan-Crispi D, et al. Cell cycle- and cancer-associated gene networks activated by Dsg2: evidence of cystatin A deregulation and a potential role in

cell-cell adhesion. PLoS One 2015;10:e0120091.
17. John Mary DJS, Manjegowda MC, Kumar A, et al. The role of cystatin A in breast cancer and its functional link with ERα. J Genet Genomics 2017;44:593-7.
18. Shiba D, Terayama M, Yamada K, et al. Clinicopathological significance of cystatin A expression in progression of esophageal squamous cell carcinoma. Medicine (Baltimore) 2018;97:e0357.
19. Duivenvoorden HM, Rautela J, Edgington-Mitchell LE, et al. Myoepithelial cell-specific expression of stefin A as a suppressor of early breast cancer invasion. J Pathol 2017;243:496-509.
20. Liu ZJ, Zheng LS, Li CZ, et al. Correlated with better prognosis, CSTA inhibits metastasis of nasopharyngeal carcinoma cells via suppressing AKT signaling through promoting METTL3 degradation. Biochim Biophys Acta Mol Basis Dis 2023;1869:166696.
21. Kumar V, Ramnarayanan K, Sundar R, et al. Single-Cell Atlas of Lineage States, Tumor Microenvironment, and Subtype-Specific Expression Programs in Gastric Cancer. Cancer Discov 2022;12:670-91.
22. Necchi A, Joseph RW, Loriot Y, et al. Atezolizumab in platinum-treated locally advanced or metastatic urothelial carcinoma: post-progression outcomes from the phase II IMvigor210 study. Ann Oncol 2017;28:3044-50.
23. Qiu X, Mao Q, Tang Y, et al. Reversed graph embedding resolves complex single-cell trajectories. Nat Methods 2017;14:979-82.
24. Jin S, Guerrero-Juarez CF, Zhang L, et al. Inference and analysis of cell-cell communication using CellChat. Nat Commun 2021;12:1088.
25. Wu Y, Yang S, Ma J, et al. Spatiotemporal Immune Landscape of Colorectal Cancer Liver Metastasis at Single-Cell Level. Cancer Discov 2022;12:134-53.
26. Luecken MD, Theis FJ. Current best practices in single-cell RNA-seq analysis: a tutorial. Mol Syst Biol 2019;15:e8746.
27. Jiang D, Turner B, Song J, et al. Comprehensive Analysis of the Unfolded Protein Response in Breast Cancer Subtypes. JCO Precis Oncol 2017;2017:PO.16.00073.
28. Galbo PM Jr, Zang X, Zheng D. Molecular Features of Cancer-associated Fibroblast Subtypes and their Implication on Cancer Pathogenesis, Prognosis, and Immunotherapy Resistance. Clin Cancer Res 2021;27:2636-47.
29. Zhu GQ, Tang Z, Huang R, et al. CD36(+) cancer-associated fibroblasts provide immunosuppressive microenvironment for hepatocellular carcinoma via secretion of macrophage migration inhibitory factor. Cell Discov 2023;9:25.
30. Smyth EC, Verheij M, Allum W, et al. Gastric cancer: ESMO Clinical Practice Guidelines for diagnosis, treatment and follow-up. Ann Oncol 2016;27:v38-49.
31. Wang R, Song S, Qin J, et al. Evolution of immune and stromal cell states and ecotypes during gastric adenocarcinoma progression. Cancer Cell 2023;41:1407-1426.e9.
32. Kim H, Hwang Y, Sung H, et al. Effectiveness of Gastric Cancer Screening on Gastric Cancer Incidence and Mortality in a Community-Based Prospective Cohort. Cancer Res Treat 2018;50:582-9.
33. Yan Y, Wang LF, Wang RF. Role of cancer-associated fibroblasts in invasion and metastasis of gastric cancer. World J Gastroenterol 2015;21:9717-26.
34. Ma M, Sun J, Liu Z, et al. The Immune Microenvironment in Gastric Cancer: Prognostic Prediction. Front Oncol 2022;12:836389.
35. Chen X, Song E. Turning foes to friends: targeting cancer-associated fibroblasts. Nat Rev Drug Discov 2019;18:99-115.
36. Zhang H, Deng T, Liu R, et al. CAF secreted miR-522 suppresses ferroptosis and promotes acquired chemo-resistance in gastric cancer. Mol Cancer 2020;19:43.
37. Shah MA, Starodub A, Sharma S, et al. Andecaliximab/GS-5745 Alone and Combined with mFOLFOX6 in Advanced Gastric and Gastroesophageal Junction Adenocarcinoma: Results from a Phase I Study. Clin Cancer Res 2018;24:3829-37.
38. Kinoshita H, Yashiro M, Fukuoka T, et al. Diffuse-type gastric cancer cells switch their driver pathways from FGFR2 signaling to SDF1/CXCR4 axis in hypoxic tumor microenvironments. Carcinogenesis 2015;36:1511-20.
39. Blaydon DC, Nitoiu D, Eckl KM, et al. Mutations in CSTA, encoding Cystatin A, underlie exfoliative ichthyosis and reveal a role for this protease inhibitor in cell-cell adhesion. Am J Hum Genet 2011;89:564-71.
40. Zhang X, Zhuge J, Liu J, et al. Prognostic signatures of sphingolipids: Understanding the immune landscape and predictive role in immunotherapy response and outcomes of hepatocellular carcinoma. Front Immunol 2023;14:1153423.

Cite this article as: Xu Q, Xue S, Zhang Y, Li J, Qian P, Zhang Y, Feng L. Identification and validation of Cystatin A as a novel promising therapeutic target for gastric cancer. J Gastrointest Oncol 2024;15(3):873-889. doi: 10.21037/jgo-23-941

